



Fractal analysis of geomagnetic data to decipher pre-earthquake process in Andaman-Nicobar region, India

Rahul Prajapati^{1*} and Kusumita Arora¹

¹ Geomagnetism Group, CSIR-National Geophysical Research Institute, Hyderabad-500007, India;
rahulphy007@gmail.com

*Correspondence: rahulphy007@gmail.com

Abstract: The emission of seismo-electromagnetic (EM) signatures prior to earthquake recorded in geomagnetic data has potential to reveal the pre-earthquake processes in focal zones. This study focused to analysis of vertical component of a geomagnetic field from Mar 2019 to Apr 2020 using fractal and multifractal approach to identify the EM signatures in Campbell Bay, a seismically active region of Andaman and Nicobar, subduction zone. The significant enhancements in monofractal dimension and spectrum width components of multifractal highlights the high frequency with less and more complex nature of EM signatures preceded by earthquakes respectively, which indicates that the pre-earthquake processes on West Andaman Fault (WAF) and Andaman Trench (AT) are due to micro fracturing. Moreover, the significant enhancements in holder exponents, components of multifractal highlight the less correlated, smooth, and low frequency characteristics of EM signatures preceded by earthquakes, which indicate that pre-earthquake processes on Seulimeum Strand (SS) fault are due to electrokinetic processes. Thus, the mono fractal, spectrum width, and holder exponent parameter respond differently to the earthquakes with different characteristics, causing EM signatures to be observed with an average of 10, 12, and 20 days prior to the earthquakes respectively, which are also lies in range of short -term earthquake prediction.

Keywords: Geomagnetic; earthquake precursor; Fractal; Andaman-Nicobar



1. Introduction

27

The existence of precursory signatures prior to an earthquake is a hotly debated topic among 28
researchers across the globe. Several convincing evidences of gas exhalations, variations in 29
groundwater level, temperature variations, fluctuations in the electric and magnetic fields, etc., 30
(Scholz et al., 1973; Rikitake, 1975; Crampin et al., 1980; Bella et al., 1995; Virk et al., 2001; Chadha 31
et al., 2008; Koizumi et al., 2004; Liu et al., 2006; Ouzounov et al., 2007; Panda et al., 1996, 2007; 32
Sethumadhav et al., 2010; Hayakawa and Molchanov, 2004), tilts the scale in favor of detectable 33
signatures of pre-earthquake phenomena. Heterogeneous lithospheric material under strain undergoes 34
micro-fracturing, which causes the polarization of charges, which in turn leads to generation of 35
electromagnetic emission and acoustic waves (Molchanov and Hayakawa, 1995). It has been 36
postulated that most crustal rocks contain dormant electronic charge carriers in the form of peroxy 37
defects, which are released under critical stress levels and flow out of the stressed sub volume as an 38
electric current, which generates magnetic field variations and low frequency EM emissions. When 39
they reach the Earth's surface, they lead to ionization of air at the ground-air interface (Hayakawa et 40
al., 1996). Observations of electromagnetic emissions prior to earthquake in frequency ranges from 41
DC, ultra-low frequency, very low frequency, electromagnetic pulses, and very high frequency 42
(Bulusu et al., 2023; Conti et al., 2021; Han et al., 2016; Hattori et al., 2013a; Hayakawa et al., 1999, 43
1996; Johnston et al., 1984) have been reported by many researchers. . Presence of precursory 44
signatures in the ULF range have been extensively studied for earthquakes of $M \geq 7$, such as Biak, 45
Spitak, Loma Prieta, Guam, Chi-Chi, Chiapas etc., (Fraser - Smith et al., 1990; Hattori et al., 2004b; 46
Hayakawa et al., 2000, 1999; Ida et al., 2008; Kopytenko et al., 1993; Molchanov et al., 1992; 47
Smirnova et al., 2013; Stanica and Stănică, 2019; Yen et al., 2004); the ULF range has received more 48



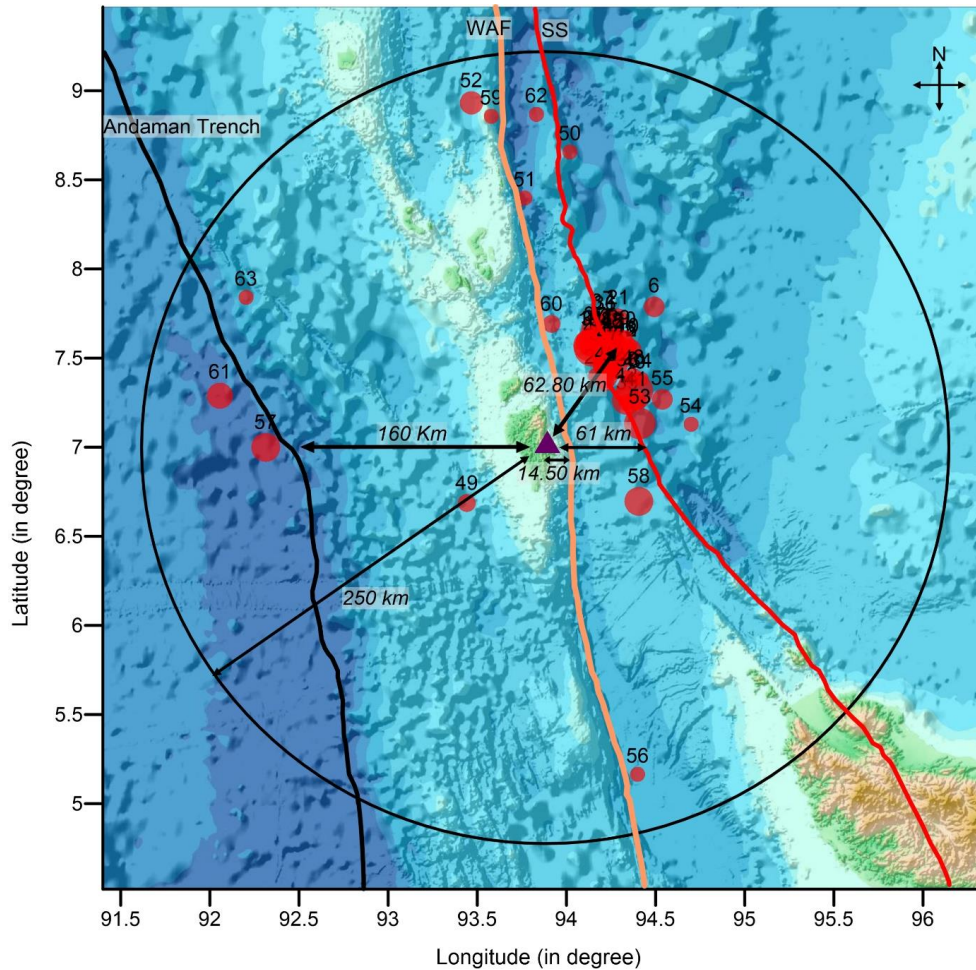
attention as they experience less attenuation and are more likely to reach the Earth's surface and 49
geomagnetic recording station. 50

Identification of the geomagnetic anomalies, which are associated with lithospheric processes is a 51
contentious issue. These variations must be uniquely identified, which are distinct from the 52
expressions of magnetospheric-ionospheric processes due to interaction with the solar wind. The most 53
preferred signal processing techniques in previous studies are polarization ratio analysis, diurnal ratio, 54
principal component analysis, singular value decomposition, mono-fractal, and multifractal analysis 55
(Bulusu et al., 2023; Gotoh et al., 2002; Hattori et al., 2004b; Hayakawa et al., 2007, 2005, 1999; 56
Rawat et al., 2016). These signal processing techniques have shown promising results in different 57
cases such as central frequency of 0.01 Hz of non-overlapping window of night time data studied by 58
Han et al. (2015), Hattori et al. (2013b), and Xu et al. (2013) used filtered diurnal signal (using db5 59
wavelet function) of target station and reference station; Han et al. (2015) has studied the diurnal ratio 60
signal from target and reference station after 15 day running mean, Han et al. (2015) have studied 61
diurnal ratio of electric as well as magnetic fields along with polarization ratio of magnetic field of 62
night time data in the ULF range, and Heavlin et al. (2022) studied the signal from a dense network 63
of stations using linear discrimination analysis (LDA) in frequency range 0.001-25 Hz. 64

The Andaman-Nicobar region is the northern part of the Sumatra subduction zone, where the Indian 65
plate is thrusting under the Burma microplate (Gahalaut et al., 2013; Meng et al., 2012; Yang et al., 66
2017). . Persistent tectonic activity is observed here along three major faults, i.e. West Andaman Fault 67
(WAF), Aceh Strands (AS), and Seulimeum Strands (SS). Some of the major earthquakes along these 68
faults have led to huge losses of life and property and continue to be a worrisome source of mega- 69
scale hazards. During Mar-2019 to Apr-2020, 63 moderate earthquakes of $M \geq 4.5$ occurred in the 70



vicinity of the geomagnetic station installed by CSIR-NGRI at Campbell Bay (CBY) in Great Nicobar 71
(Figure 1). Hayakawa et al. (2005) have examined the 3-component data from the same station to 72
identify the anomalous signatures in the polarization ratio of the ULF geomagnetic signal and the 73
diurnal ratio of the Z component for these moderate earthquakes and found a correlatable pattern of 74
these signatures with earthquake occurrence in 75% of the events. This encouraged a deeper 75
investigation into the possible causes of these patterns. The property of Self Organized Critically 76
(SOC) of earthquakes provides the motivation to study the fractal characteristics of the geomagnetic 77
time series to decipher the nature of the anomalous signatures in the data (Bak et al., 1988; Hayakawa 78
et al., 1999). 79



81

Figure 1. Bathymetry map of Andaman-Nicobar subduction zone including Sumatran Fault System; i.e. 82
Seulimeum Strand, West Andaman Fault and Andaman Trench (modified after Cochran 2010; E. Anusha 83
et al., 2020). The circles are representing the earthquake's location and magnitude (size of circle) 84
correspond to each fault system. 85

86

In the case of the Guam earthquake, 1993, found a significant change in scaling exponent prior to the event 87
(Hayakawa et al., 1999). A similar behavior of scaling exponent was also observed prior to the Biak 88
earthquake in 1996 (Hayakawa et al., 2000). Fractal nature is tested with different approaches (Higuchi, 89



1988); the Higuchi method provides more consistent and reliable fractal dimension value for the study of 90
fractal behavior of ULF signal (Hattori et al., 2004a; Gotoh et al., 2003; Smirnova et al., 2004). Further, 91
multifractal techniques can better represent the different sources of the signals associated with seismicity 92
(Turcotte, 1989). 93

In this study, we will use nighttime Z-component geomagnetic signal as it is more sensitive to changes in 94
local EM emissions, which are likely to be generated by microfracturing and associated lithospheric 95
deformation. We propose to compute the fractal and multifractal dimensions of the data to extract signatures 96
of more intense perturbations of the signal represented by higher fractal dimension values. The anomalous 97
EM emissions can be correlated with earthquake events in search of pre-earthquake signatures. The 98
earthquake catalog (Table T1) of the study region is adopted from the International Seismological Centre 99
(ISC) with $M \geq 4.5$ and epicenter within 250 km radius of recording station. 63 earthquakes are recorded 100
from 31 March 2019 to 24 April 2020. 101

2. Methodological Approach 102

It is proposed to apply both fractal and multifractal approaches to the Z component time series, to distinguish 103
between the different source characteristics and examine their relationship to earthquake parameters. The Z- 104
component of 1 Hz geomagnetic signal analyzed because it is more prone to sense or affected by the local EM 105
field from lithospheric deformation in which vertical components are dominated. 106

- (i) Examination of fractal and multifractal behavior of Z-component for one-day data using Higuchi method 107
and wavelet leader technique, respectively. Gotoh et al. (2003) tested different methods for estimation 108
of fractal dimension of geomagnetic signal and suggested that the fractal dimension value using Higuchi 109
method, provided in equation as below, is more reliable and consistent than others. Application of 110



Higuchi method on one day nighttime (22:00-02:00 LT) Z-component of geomagnetic signal of 3 April 111
2019, is shown in Figure 2. 112

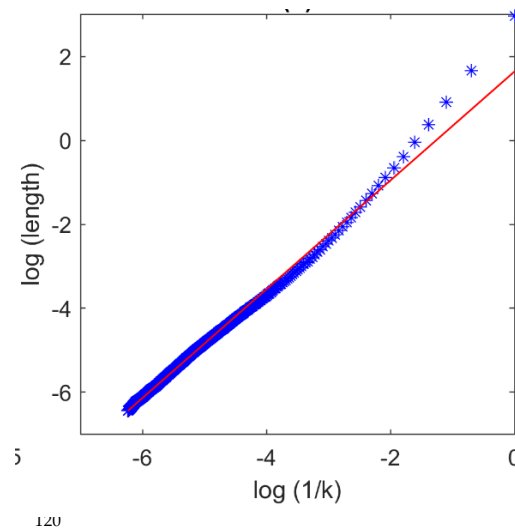


Figure 2. The linear fitting over and log of wavenumber and (b) log of measured length log of 1/scale, shows 121
the power law nature of geomagnetic signal. 122

(i) Muzy et al. (1994) proposed an approach for multifractal analysis based on discrete wavelet. Larger the 124
width of multifractal spectrum indicates larger the multifractality or intermittency, and vice-versa. The 125
width of multifractal spectrum h_w (from $-q$ to $+q$) indicates the overall degree of multifractality of 126
signal. The spectrum width h_{wp} ($q > 0$) and h_{wn} ($q < 0$) indicates the weaker and stronger singularity 127
of multifractal signal. The $h_{max}-h_{min}$ curve defines the average fluctuations embedded in the signal 128
while $h(0)$ represents the zero-order exponent or monofractal dimension (Hayakawa et al., 1999). 129
Similarly, f_{max} define the exponent which occurred maximum number of times. Application of 130
multifractal on one day nighttime (22:00-02:00 LT) Z-component of geomagnetic signal of 3 April 2019, 131
is shown in Figure 3. 132

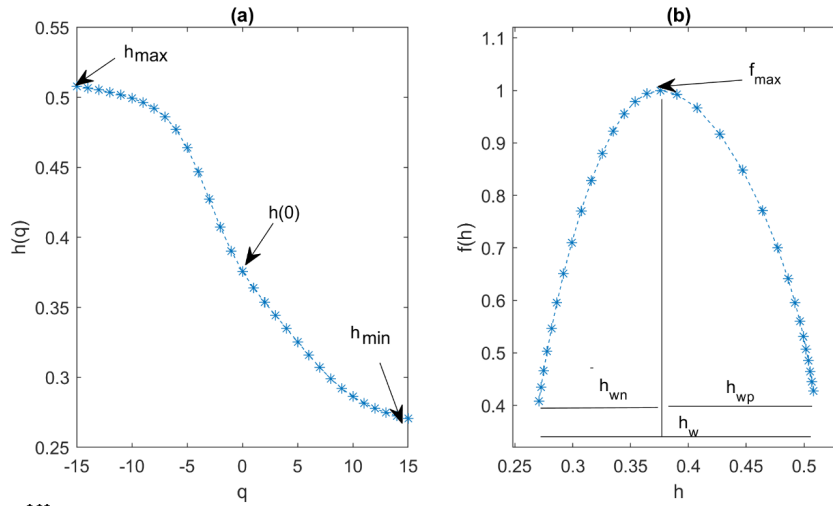


Figure 3. The multifractal analysis for 1800 samples of 3rd April 2019, where (a) The variation of holder exponent (h) with moment order q in range of -15 to $+15$ showing as h_{min} , h_{max} , and $h(0)$. (b) Multifractal spectrum showing the width of spectrum h_w , h_{wp} and h_{wn} .

- (ii) The high correlated values measured from fractal, is reason to select the Higuchi method, while for multifractal, wavelet leader is selected due to contact support for wide range of q ($-q$ to $+q$) and stability for scaling function for negative q values compared to other techniques. From fractal, the power law behaviour, and from multifractal, the finite width of multifractal spectrum and variation in holder exponent indicates the fractal and multifractal nature of signal, respectively.
- (iii) The fractal dimension f_D of the total duration of Z-component data is calculated for consecutive time windows of 30 min to trace the variations of the fractal dimension, producing eight values for each day. The choice of a 30 min time window (consisting of 1800 data points) is based on the balance between the stability of fluctuations in fractal dimension and minimizing loss of information after trials with 15 min and 1 hr. time windows.



- (iv) Similarly, the spectrum width parameter (h_w , h_{wp} , and h_{wn}) and holder exponent parameter h_{max} , h_{min} and, $h(0)$ estimated for the total length of Z component from window of 30 minute to identify the degree of singularity or complexity (global, weaker, and stronger) as well as degree of fluctuations with respect to amplitude (from smaller to larger). The shorter fluctuations in fractal dimensions are smoothed by applying a 15-day moving mean.
- (v) The increments in fractal dimension and multifractal parameter (spectrum width and holder exponent) value greater than the threshold value ($\mu + \sigma$) are considered as a significant increment as evidence of existence of EM signatures from lithospheric deformation.

3. Results

3.1 Monofractal analysis

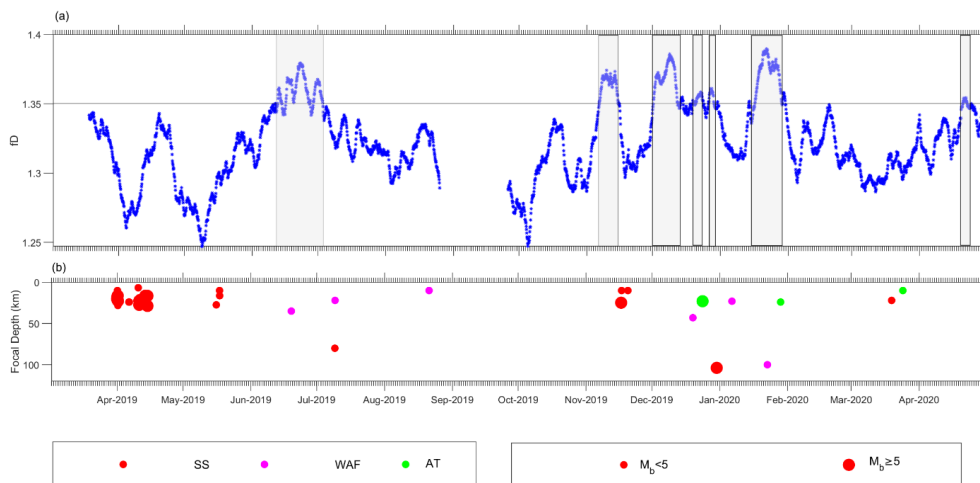


Figure 4. (a) Temporal variation of fractal dimension estimated from Higuchi method (15 days moving mean) of Z-component of geomagnetic signal. (b) The time line earthquake occurrences in same duration of geomagnetic signal.



The temporal variations in f_D of vertical component of geomagnetic signal are shown in Figure 4a; f_D 170
greater than the threshold value 1.35 (defined by $\mu + \sigma$) are indicated by grey color rectangles. These 171
enhanced values possibly represent the additional complexity in the signal caused by pre-earthquake 172
microfracturing. The observed enhancements in f_D and corresponding earthquakes are summarized in Table 173
T2. For the earthquake swarm of 1-18 Apr, 2019, and the three earthquakes of 16 & 17th May, 2019, no 174
preceding or coinciding enhancements are recorded. Two phases of enhancements during 12-13 and 16-19 175
Jun, 2019 occur prior to earthquake of 19th Jun, 2019 ($M=4.6$ of focal depth of 35 km, along the WAF with 176
epicentral distance of 60 km). The enhancements during 20-26 Jun, and 29 Jun-2 Jul 2019 occur before the 177
dual earthquakes of 9-Jul, 2019 ($M=4.5$ -fd 80 km-epicenter distance 185 km along SS fault; $M=4.5$ -fd 22 178
km epicenter distance 156 km along WAF). No enhancements beyond threshold value are recorded prior 179
to the very shallow 10 km depth earthquake of 21 Aug ($M=4.8$) with epicenter 219 km away along the 180
WAF. During Sept and Oct, 2019 neither earthquakes nor enhanced fractal dimensions are observed. Three 181
earthquakes occurred in November, two on 17th and one on the 20th, all on the SS fault. They were of M 182
5.1, 4.5, 4.7 respectively at shallow focal depths and corresponding epicenters at 60, 91, 78 km from 183
recording site. These events are preceded by a long duration enhancement in fractal dimension from 6-15 184
Nov. In December, three earthquakes occurred on 19th, 24th and 30th of magnitudes 4.5, 5, 5 respectively on 185
the WAF, AT and SS faults respectively. The earthquakes of 19th Dec of focal depth 43 km and despite 186
large epicentral distance of 212 km from recording site, was preceded by a large amplitude and long 187
duration enhancement of fractal dimension 1-14 Dec; for the next two earthquakes of focal depths 23 and 188
104 km and corresponding epicentral distances of 173 and 67 km minor enhancements were observed 189
during 18-23 Dec and 26-28 Dec. For the three earthquakes of Jan 2020, the M 4.5 shallow earthquake of 190
6th Jan with epicentral distance >200 km, no enhancements are observed. The earthquakes of 22nd and 28th 191



Jan occurred. No earthquakes were recorded in Feb 2020 and no anomalous enhancements are observed. 192
During March 19th and 24th there were two shallow M=4.5 earthquakes with epicentral distances more than 193
200 km along the SS and AT respectively. During 20-22 Apr, a small enhancement is observed, the 194
succeeding earthquake is not included in present catalogue. 195

3.2 Multifractal analysis 196

The holder exponent curve and multifractal spectrum width are calculated for the same data of 3rd April, 197
2019 for the 30 min interval 22:00 – 22:30 LT, with 1800 data points. The large variation in Hurst exponent 198
against moment order q (Figure 4a) and wide width of multifractal spectrum of geomagnetic time series 199
(Figure 4b) indicate the multifractal nature of geomagnetic signal. The multifractal behavior of a signal is 200
generally characterized by the width of multifractal spectrum (h_w) as well as spectrum width h_{wn} 201
correspond to $-q$ to 0 and h_{wp} correspond to $+q$ to 0 also assist in characterizing the specific nature of the 202
geomagnetic signal (Figure 4). Apart from spectrum width parameter, holder exponent parameters, such as 203
 h_{min} , h_{max} , $h(0)$, and f_{max} are also useful to characterize the nature of pre-earthquake geomagnetic signal 204
(Figure 4). 205

3.2.1 Multifractal spectrum width 206

The width of multifractal spectrum (h_w , h_{wp} and h_{wn}) of a sliding window of 1800 data points (half an 207
hour) without overlapping is computed for whole time series of vertical component of Z-component (Figure 208
5). The 15-day moving mean of variation in spectrum width of multifractal spectrum shows significant 209
variations in the range of 0.09 to 0.26. The enhancement greater than threshold value ($\mu + \sigma$) are considered 210
as a significant enhancement in fractal dimension. In examining of enhancement in h_w , h_{wp} and h_{wn} 211
component, the enhancement in least one component among all are considered as significant enhancement 212
indicating the perturbation in geomagnetic signal (Figure 5). The enhancements in h_w , h_{wp} and h_{wn} 213



component with corresponding earthquakes is summarized in Table T3. For the earthquake swarm of 31 214
Mar-18 Apr, 2019 (moderate magnitude 4.5-5.3, shallow focal depth 15-30km, and epicentral distance 50- 215
100 km), a preceding enhancement (in h_w , h_{wp} , and h_{wn}) component occurred during 17-22 Mar, 2019. 216
The significant enhancement during 14 May (in h_w component), 14-15 and 17-20 May, 2019 (in h_{wp} 217
component) and 29Apr-5 May, 2019 (in h_{wn} component) are partly common to each other and occurred 218
prior, co and post of earthquake 16th and 17th May, 2019 (moderate magnitude (4.5-4.8), focal depth (10- 219
27.4), and epicentral distance (58-71)). The two sets of enhancement during 22-25 May, 2019 and 4-22 220
Jun, 2019 (in h_w and h_{wp}) and one persistence enhancement during 8-22 Jun, 2019 occurred prior to 221
earthquake 19 Jun, 2019 (M 4.6, focal depth 60 km, and epi. Dist 60 km). the enhancement in common 222
duration 30-9th Jul, 2019 (different duration of persistence) and no enhancement in h_{wn} component 223
occurred prior to two earthquakes 9th Jul, 2019 at two different locations with moderate magnitude (4.5), 224
moderate and shallow focal depth (80 and 22 km) and large epicentral distance (185 and 156 km). The 225
common enhancement during 17-19th Jul, 2019 in h_w and h_{wn} component (not same duration of 226
persistence) occurred prior to earthquake on 21st Aug, 2019 (M 4.8, focal depth 10 km, and large epicentral 227
distance 219 km). the common enhancements during 9-15 Oct, 2019, 7-10th Nov, 2019, in h_w and h_{wp} 228
component, 11-12th Nov in h_w , and 2-3, 12-14th Nov, 2019 in h_{wp} component occurred prior to earthquake 229
17th and 20th Nov, 2019 with moderate magnitude (4.7-5.1), focal depth (10-25 km), and epicentral distance 230
(60-91 km). Further, the four-earthquake occurred during December, 2019 and 1st week of Jan, 2020 is not 231
(moderate magnitude, moderate focal depth, and moderate to large epicentral distances) preceded by any 232
significant enhancement in components of multifractal width parameter. The common enhancement during 233
16-20 Jan, 2020 in h_w and h_{wp} component occurred prior to earthquake 22nd (M 4.6, focal depth 100km, 234
and epicentral distance 77) and 28th Jan, 2020 (M 4.9, focal depth 24km, and epicentral distance 204 km). 235



Further, the two-earthquake occurred in May-2020 (moderate magnitude, shallow focal depth, and large epicentral distance) is not preceded by any enhancement in components of multifractal width parameter. 236
 237

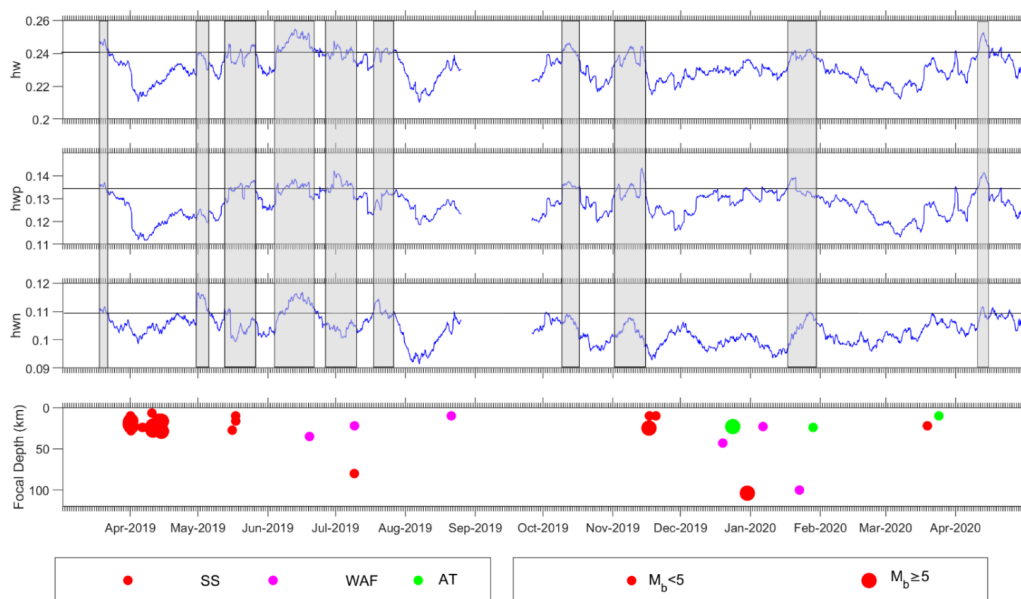


Figure 5. Temporal variation in spectrum width h_w , h_{wp} and h_{wn} from top panel and anomalous behavior 238
 are highlighted by grey color. The bottom panel showing the occurrences of earthquake with magnitude 239
 (size of circle) and corresponding faults (different color). Top four panel showing the detail view of Jun 240
 2019 month. 241
 242

3.2.2 Holder Exponent 243

The holder exponent parameter (h_{max} , h_{min} , $h(0)$, and f_{max}) used for defining the multifractal spectrum 244
 curve also shows significant variations in the amplitude and enhancements greater than threshold value 245
 (1.0082, 0.4626, 0.5873, 0.3612) are treated as significant (Figure 6). The enhancements in h_{max} , h_{min} , 246
 $h(0)$, and f_{max} components with corresponding earthquakes are summarized in Table T4. 247
 248

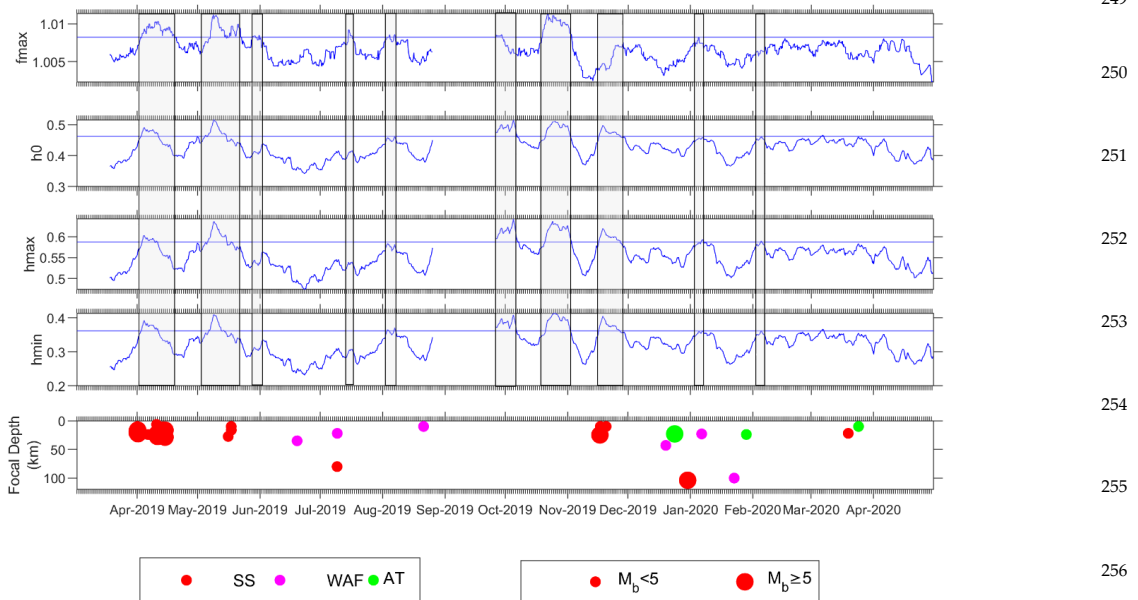


Figure 6. Temporal variation in holder exponent parameters i.e. f_{max} , h_{fmax} , h_{max} and h_{min} from top panel and anomalous behaviour are highlighted by grey colour. The bottom panel showing the occurrences of earthquake with magnitude (size of circle) and corresponding faults with different color.

The common enhancements during 2-18 April, 2019 in all components of holder exponent are coincide with the swarm of earthquake 31st 18th April, 2019 with moderate magnitude, moderate focal depth, and moderate to large epicentral distance. The next common enhancements noted during 6-14 May, 2019 in all components of holder exponent occurred prior to the three earthquakes (moderate magnitude, focal depth and epicentral distance), one 16th May, 2019, and two 17th May, 2019. For the same earthquake two small co and post seismic enhancement noted in f_{max} component during 17-19 May, 2019. The small enhancement in only f_{max} component during 20-21 May, 2019 is preceded by the earthquake 19th Jun, 2019 with moderate magnitude, focal depth, and epicentral distances. Further, the two-earthquake occurred on 9th July with moderate magnitude, epicentral distance, large epicentral distance and different location is



not preceded by enhancements in any component of holder exponent. Further, the two small enhancements 269
during 15-16 Jul, and 6 Aug, 2019 in f_{max} component and two small enhancements in h_{min} during 6 Aug, 270
2019 are occurred prior to the earthquake 21 Aug, 2019. The two enhancements common in all components 271
but different duration of persistence, one small during 26 Sep-5Oct, 2019 and persistence during 16 Oct-24 272
Nov, 2019 occurred prior as well as coincidence and post to the three earthquakes. Two on similar location 273
17th Nov, 2019 and one on different location 20th Nov, 2019 with moderate magnitude, shallow to very 274
shallow earthquake, and moderate epicentral distance. Further, the three-earthquake occurred in December, 275
2019, the first two with moderate magnitude and focal depth and large epicentral distance and third with 276
moderate magnitude, large focal depth, and moderate epicentral distance are not preceded by enhancement 277
in any component of holder exponent. The next one small enhancement in h_{max} component only during 3- 278
8 Jan, 20020 is coincide with earthquake 06th Jan, 2020 (mod. Magnitude, mod. Focal depth, and large 279
epicentral distance) and preceded by two earthquakes occurred on 22 and 28th Jan, 2020 (with moderate 280
magnitude, moderate and large focal depth; large and moderate epicentral distance). 281

For the earthquake swarm of 31 March, 2019 and early April, the spectrum width shows a small 282
enhancement during 17-20th March, that is 12 days prior to the earthquake cluster, which have magnitudes 283
between 4.5 to 5.3 and occur in a small region along the SS fault. There is no enhancement of the Holder 284
exponent. For the intermittent earthquakes in mid-April, there is no signal in the spectrum width but the 285
Holder exponent shows a consistent enhance during 3-10 April, a week before the main cluster. In early 286
May, upto 5th, h_{wn} shows an enhancement; the pattern is mimicked in the Holder exponent without crossing 287
the threshold value. Small anomalous enhancements 12-14th May on the h_{wn} , h_{wp} and h_w of spectrum 288
width, just prior to the moderate earthquakes on 16th and 17th May. The holder exponent exhibits a longer, 289
more consistent enhancement during 7-14th May, fmax shows co-seismic anomaly on 17-19 May, followed 290



by on 20-21 May. Post seismic perturbations are also noted in the spectrum width. For the M4.6 earthquakes 291
of 19th June, long duration anomalies are seen in spectrum width but not in Holder exponent. For the dual 292
earthquakes on 9th July, pre and post seismic anomalies are seen in spectrum width; only one 14-16 June 293
anomaly is seen in Holder exponent. There is no significant multifractal anomaly for the 21 Aug, very 294
shallow earthquake. In October 2019, significant repeated anomalies are observed in Holder exponent right 295
till Nov, 2019. In the second half of Jan and much of February well extended, there are several stand-along 296
earthquakes; no significant enhancement is observed for any of these earthquakes. A short enhancement 297
can be noted in 11-14 April, which may be used to forecast the next event. 298

3.3 Combined result of monofractal and multifractal analysis 299

Figure 4, 5, and 6, clearly states that the all components from monofractal and multifractal, has different 300
response for each earthquake, indicating different characteristics of signal, which can be used as indicator 301
of pre-earthquake processes in the focal zone of earthquake. In this regard, we have characterized the 302
enhancements of components in three types of patterns: (i) present in only monofractal component, (ii) 303
present in only multifractal components, and (iii) present in monofractal as well as in multifractal 304
component. 305

The significant enhancement from both parameter (monofractal and multifractal) with corresponding 306
earthquake from figure 4, 5, and 6 is summarized in Figure 7. 307

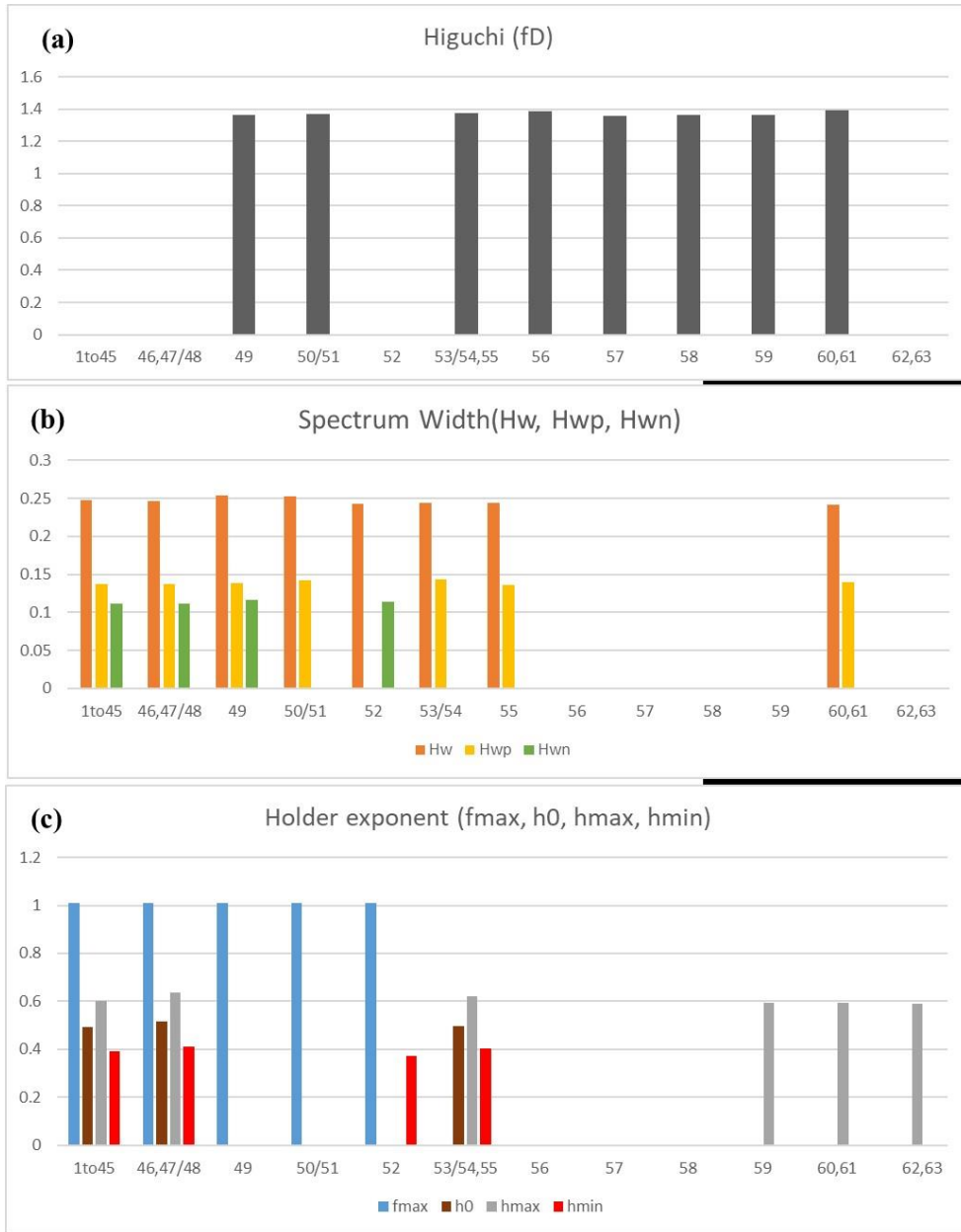
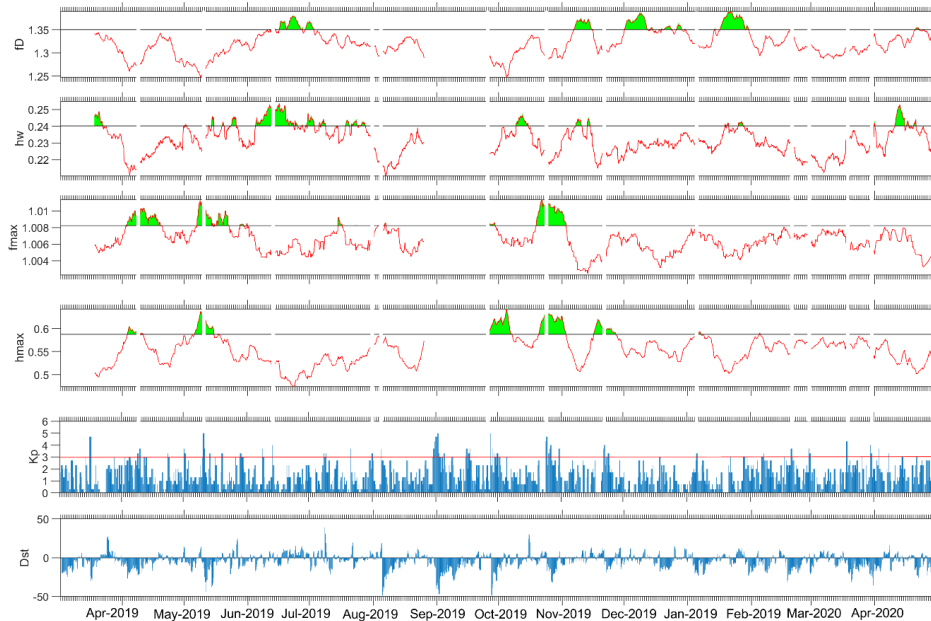


Figure 7. The components of significant enhancement with corresponding earthquakes from (a) Higuchi fractal dimension, (b) Spectrum width, and (c) Holder exponent.



Figure 7 deciphers that the Higuchi fractal dimension from monofractal parameter, exhibit the significant 329
enhancements corresponds to earthquake 56, 57, and 58, while there are no enhancements in multifractal 330
component correspond to same earthquake. Furthermore, there are significant enhancements in multifractal 331
components correspond to the earthquake 1-45 (swarm of earthquake), 46, 47/48, 52, 62, and 63, while 332
there are no enhancements in monofractal component (or Higuchi fractal dimension) correspond same 333
earthquakes. Additionally, it is also noted that the earthquake 1-45, 46, 47/48 exhibit to all component of 334
spectrum width (h_{wn} , h_{wp} and h_w) and holder exponent f_{max} , h_{max} , h_{min} , and $h(0)$, while for earthquake 335
52 (h_w , h_{wn} , h_{min} , and f_{max}), 62 (h_{max}), and 63 (h_{max}) all components of multifractal parameters are not 336
present. Similarly, the significant enhancements correspond to earthquakes 49, 50/51, 53/54, 55, 59, 60, 337
and 61 observed in monofractal as well as multifractal components, but not in all components of 338
multifractal. Apart this, from multifractal parameter it is also noted that, h_w component of spectrum width 339
is common to each enhancement, while h_{max} component of holder exponent is common to each 340
enhancement except three instances correspond to 49, 50/51, and 52 earthquakes whereas f_{max} is present 341
to the same earthquake. 342

The data analyzed for a duration of 14 months have strong possibility to be affected with magnetospheric 343
and ionospheric effect, which may also appear as a significant enhanced signature in the present analysis. 344
Thus, the night time data for 4-hour (23:00 to 02:00) chosen for study, to minimize interference of global 345
field (from ionosphere), while the interference of magnetosphere during disturb days may still present in 346
data, which can be easily traced by placatory index Kp and Dst. From the observation 347



357

Figure 8. Temporal variation of (a) Higuchi fractal dimension, (b) spectrum width component of 358
multifractal width parameter, (c) fmax component, and (d) hmax component after removing the data 359
correspond to (f) $Kp > 3$ and (g) $Dst < -50$. 360

of Kp and Dst index, the Kp index greater than 3 and Dst index smaller than -50 are present for very short 362
duration and very less frequent, which effect are diminished considerably after averaging of each 363
component with 15 day moving mean (Figure 8). Thus, after removing the data points of correspond to Kp 364
greater than 3 and Dst less than -50 from each component the significant enhancements may reflect the 365
seismogenic effect from Earth's subsurface (Figure 8). An additional component of diurnal ratio is also 366
appended for correlation with monofractal and multifractal components, which is also treated with criteria 367
of planetary index (figure 8). 368



Therefore, from multifractal analysis, h_w , h_{max} , and f_{max} components, and Higuchi fractal dimension from 369
monofractal parameter has traced all the significant signatures corresponding to the seismogenic activity in 370
the earthquake. The month-wise analysis from Mar-2019 to April -2020 of each component preferred for 371
detail analysis of enhancements shown in Figure S1-S14. 372

Discussion: 373

We examine the combined observations of signatures from monofractal or Higuchi fractal dimension (f_D) and 374
multifractal components (h_w , h_{max} and f_{max}) along with diurnal ratio to unravel a linked pattern, which can 375
be interpreted as related to earthquake processes (Figure 9). 376

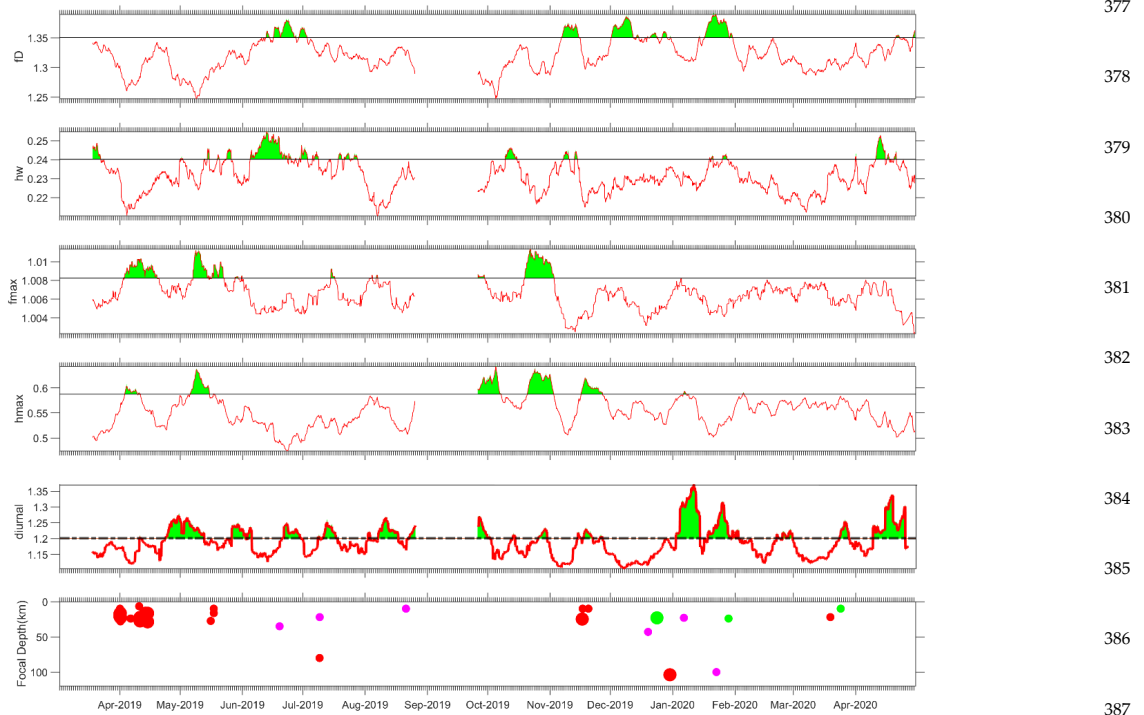


Figure 9. The significant enhancement in temporal variation of (a) Higuchi fractal dimension, (b) spectrum 389
width component of multifractal width parameter, (c) f_{max} component showing the holder exponent 390



presence highest number of time (d) h_{max} component showing the largest value of holder exponent, and 391
(e) diurnal ratio, indicated by shaded green color, (f) the occurrences of earthquakes in same time duration 392
with magnitude and focal depth. 393

A swarm of earthquakes (1-45 as per our catalogue) along the SS fault occurred around the first week of April 395
2019. The data is available from 15th March and no anomalies were identified in the Diurnal ratio; hence it 396
was concluded that data length was insufficient (Prajapati and Arora, 2024). While no anomalies were detected 397
in the f_D , distinct enhancements are noted in the Spectrum width 14 days prior to the beginning of the swarm. 398
Co-seismic f_{max} over the entire duration and muted h_{max} enhancements are noted during 2-18 April and 2- 399
10 April respectively. 400

For the moderate magnitude, shallow focus earthquakes 46, 47, 48, clustered close together during mid-June 401
2019, Diurnal ratio shows a significant enhancement 50 days before the events, whereas no anomalies are 402
recorded in f_D . Enhancements in both h_{max} and f_{max} start 11 and 9 days before the events and continue co- 403
seismically. 404

Earthquake 49 on 19th June 2019 was of moderate magnitude, moderate focal depth and moderate epicentral 405
distance on the WAF. It is preceded by small enhancement in Diurnal ratio 22 days before, f_D 7 days prior 406
and continues co-seismically. Spectrum width enhancement starts 15 days prior to event, which continues co- 407
seismically, there are no signatures in h_{max} or f_{max} . 408

The dual earthquakes 50 and 51, occurred soon after 49, at large epicentral distances on the WAF (shallow 409
focal depth) and on the SS (deep focal depth) in opposite directions to the recording station. Diurnal ratio 410
shows a significant anomaly 16 days prior to the event, accompanied by slight increase in f_D 19 days before. 411
Mild perturbations are also observed in Spectrum width 9-4 days before the events. 412



The earthquake 52 is similar to 49, with shallower focal depth and very large epicentral distance of 219 km 413
on the WAF. It is preceded by enhancement in Diurnal ratio is seen 14 days before, no signatures are seen in 414
any other parameter. 415

The earthquakes 53, 54, 55 on 17 and 20 Nov 2019, occur along the SS fault with moderate epicentral distances 416
and shallow focal depth; 53 has magnitude of 5. They are preceded by two phases of small enhancements in 417
Diurnal ratio 21 and 3 days before the earthquakes, continuing to co-seismic signatures. Enhancements in 418
 h_{max} continue to co-seismic signatures. Signatures in h_w are very muted, f_D shows significant enhancement 419
2 days prior to the earthquakes. 420

Earthquakes 56-63 are individual events, from end of 2019 to first quarter of 2020, separated by several days 421
to weeks intervals in between. Earthquake 56 has very large epicentral distance, also occurring on the WAF 422
like earthquake 52, but with a focal depth of 43 km. This is followed by 57, which is a M=5 earthquake at 423
very shallow focal depth, at large epicentral distance on the AT. 58 occurred on Dec 30, 2019, an M=5 event 424
on the SS fault with large focal depth and moderate epicentral distance. The events are preceded by a 425
significant enhancement in f_D , but no other signatures. With only one station, it is not possible to construct an 426
earthquake-anomaly link for this scenario. The cluster of 53-54-55, for which signatures are noted in Diurnal 427
ratio, f_D , and h_{max} , occurred in a closer duration period, on the same SS fault at moderate epicentral distances 428
and are also at shallow focal depth. The earthquake 59 is of moderate magnitude, shallow focal depth but large 429
epicentral distance on the WAF. Curiously, a co- and post seismic enhancement in diurnal ratio is the sole 430
signature for this event. For the earthquakes 60 (large focal depth and moderate epicentral distance on the 431
WAF) and 61 (shallow focal depth and large epicentral distance on the AT), co-seismic enhancement in 432
diurnal ratio is accompanied by similar enhancement in f_D . Earthquakes 62 (moderate magnitude, shallow 433
focal depth and large epicentral distance on the AT) and 63 (moderate magnitude, shallow focal depth and 434



large epicentral distance also on the AT), no preceding signatures are observed on any of the parameters. 435

However, a distinct post seismic increase in diurnal ratio is noted. 436

In April 2020, enhancements in h_w during 10-14 April and Diurnal ratio during 10-24 April are observed. 437

Several research articles are available (Hayakawa et al., 1999; Gotoh et al., 2003; Ida et al., 2012) to study the 438

behavior of geomagnetic signal using non-linear signal processing techniques such as monofractal and 439

multifractal in context of EM field generated from local sources due to seismogenic activity. Hayakawa et al. 440

(1999) have analysis on H, D, and Z component of ULF geomagnetic signal recorded at 65 km from the 441

epicenter of Guam earthquake with M8 occurred on 8th Oct, 1993 at focal depth of around 60 km carried using 442

fractal (spectral method) and Hurst exponent analysis (rescaled scaled range R/S method). They inferred that 443

decreasing value of slope (β) from 2.5 to ~ 1 before the earthquake, which can be considered as an indicator 444

of SOC, where $\beta \sim 1.1$ is critical value prior to the earthquake. However, no significant changes observed in 445

Hurst exponent by R/S analysis. The large-scale variation and decrease in ULF spectrum slope (or increase in 446

fractal dimension) means increase high frequency fluctuations is a proxy measure of small-scale fractal 447

structure cause by active microfracturing process followed by generation of seismogenic ULF emission. In 448

our study, we have also noticed the increase in fractal dimension atleast 10 days prior to the earthquake (49,50- 449

51,53-55, and 60-61) with moderate magnitude ($4.5 < M < 5.1$), shallow and moderate focal depth (35, 51,14, 450

and 62km), as well as small, moderate, and large epicentral distance (60, 170, 76, and 140km). The increasing 451

fractal dimension before the earthquakes are suggests the microfracturing process in Earth's crust to be the 452

cause of generation and emission of EM field in the vicinity of recording station. 453

Gotoh et al. (2003) have analyzed the ULF geomagnetic data recorded at three stations on Izu peninsula, 454

Japan, where a nearby strong earthquake swarm started from 26, June to August 2000 with magnitude upto 455

6.5. An eruption of volcanic also started simultaneously in Miyakejima Island. Izu region on Philippine plate 456



is under tensile stress and seismically very active because of subduction of Pacific plate at Nankai and Sagami 457
Troughs (Uyeda et al., 2002). The monofractal dimension of the H component shows an increase a week 458
before the earthquake. In present study, we have analyzed Z-component instead of H-component, because 459
recent studies suggested that Z-component is more sensitive for EM fields generated from local sources. In 460
our study we did not find any significant signature of enhanced fractal dimension of Z component one week 461
prior to a swarm of 45 earthquakes from 31-Mar to 18-April, 2019, however an enhancement in spectrum 462
width parameter (h_w), 10 days before the swarm activity started. 463
Further, (Ida et al., 2005) carried out the multifractal analysis on H component of geomagnetic signal recorded 464
at 65 km from the epicenter of Guam earthquake occurred on 8th Oct, 1993 at focal depth of around 60 km. A 465
westward movement of the Pacific plate and its subduction under Philippine plate triggered the Guam 466
earthquake (Ms 8.0) at shallow dipping subduction zone with a strike slip fault along the trench (Harris, 1993). 467
Ida et al. (2005) found significant changes in the multifractal parameters of Holder exponent and spectrum 468
width (α_{min} , α_{max} , w , Δ , f_{max} , $\alpha(f_{max})$, and D_q , for $q < 0$, $q > 0$, and $q = 0$). The observation of 9 days 469
running mean of spectrum width w and α_{max} shows clear and significant variation 30 days prior to the 470
earthquake. In our analysis of multifractal parameters from moderate subduction zone earthquakes, with focal 471
depth in range of 10-30 km, the 15-day running mean of Spectrum width and Holder exponent show significant 472
enhancements 12 and 20 days prior to those earthquakes, which occurred close in time as a cluster (1-45, 47- 473
48, 50-51, 53-55). This difference in pattern may be due to the large differences in magnitude of the studied 474
earthquakes. 475
Ida et al. (2012) analyzed the fractal dimension (estimated by Higuchi method) of ULF data recorded at Kashi 476
station, China, approximately for four years (Mar, 2003 to Dec, 2006), in which several moderate earthquakes 477
occurred (greater than 5.0 and close to 6) at epicentral distances of 100 to 125, including one earthquake at 478



approximately 300 km. The region is seismically very active due to relative movement of plates along SAF 479
fault (normal fault) is locally dominant in the area (He et al., 2015). Ida et al. (2012) applied the criterion of 480
 $\mu \pm 2\sigma$ to define the significant variations of the fractal dimension and reported decrease in the Z component 481
for two earthquakes (M 5.7 and M 5.4) while earthquakes with magnitude greater than 5 did not show any 482
signature. The enhancement in f_D is interpreted as indication of dominance of high frequency component and 483
decrease in f_D as dominance of low frequency component, which may correlate with the high frequency 484
mechanism like micro-fracturing and slow processes like electrokinetic effect respectively. Potirakis et al. 485
(2017) has analyzed geomagnetic data (H, D, and Z) at station Kakioka (KAK) at epicentral distance of 300 486
km from Tohoku earthquake (M 9.0) of 11 March, 2011. The earthquake was caused by the rupture of a stretch 487
of the subduction zone associated with the Japan Trench, which separates the Eurasian Plate from the 488
subducting Pacific Plate. The data analyzed using DFA and Higuchi method, observed a significant decrease 489
in spectral exponent (using DFA) and corresponding increase in fractal dimension (using Higuchi method) 5- 490
6 months prior to the large magnitude Tohoku earthquake. In our study, we have found significant 491
enhancements with the criterion of $\mu + \sigma$, producing pre-seismic increases in f_D for multiple earthquake 492
occurrences (50-51, 53-55) with $4.6 < M = 5$ and either shallow focal depth or small epicentral distance, 19 and 493
11 days before the earthquakes. 494

In our work, we have applied both mono and multifractal analysis to the geomagnetic Z component data, the 495
differences in the trends of the fractal parameters reveal interesting inferences (Table 1). We have defined 496
four clusters of the earthquakes under study (1-45, 47-48, 50-51, 53-55). There are 10 earthquakes, which 497
occurred as single events. For the single events 52, 56-63 ($4.5 < M < 5.0$), which are characterized by either large 498
focal depth (>100 km) or large epicentral distance (~ 200 km), signatures in multifractal parameters. We infer 499
that the EM fields from such moderate magnitude and large epicentral distance earthquakes are too weak to 500



detect by multifractal and diurnal ratio approach. For the same single events (with focal depth >100km or 501
epicentral distance ~200 km), we observed that enhancements in f_D corresponding to earthquakes 56,57,58, 502
60, and 61 while the earthquake 52, 59, 62, 63 are not correspond to any pre-co or post enhancements in f_D 503
parameter. The significant enhancement corresponds to 5 events out of 9, including two co-seismic signature 504
(60 and 61) indicate the greater efficacy of f_D parameter than multifractal parameter for single events with 505
focal depth >100km or epicentral distance ~200 km. The earthquake 52 is associated with an increase in the 506
Diurnal ratio 13 days in advance. The single event 49 is characterized by moderate focal depth and epicentral 507
distance, which is associated with co-seismic enhancements in f_D , pre-seismic signatures in h_w (7 days prior) 508
and diurnal ratio (15 days prior). 509

The clusters, on the other hand, produce prominent signatures in the multifractal parameters. The first cluster 510
(1-45) has signature in h_w (14 days prior) and a co-seismic enhancement in f_{max} . The second cluster (47-48) 511
has signatures in f_{max} , h_{max} and diurnal ratio, 9, 9, 13 days prior to event respectively. The third cluster (50- 512
51) at a larger epicentral distance of 165 km, has signatures in f_D , h_w and diurnal ratio 19, 9, 19 days prior to 513
event respectively. The fourth cluster (53-55) includes earthquakes of $M=5.1$ and the events are at shallow 514
focal depth and small-to-moderate epicentral distances produce signatures in f_D and all the multifractal 515
parameters as well as diurnal ratio. 516

The combined observation from fractal (mono and multifractal) and diurnal ratio (Table 1) clearly indicates 517
that the fractal parameters exhibit significant enhancement associated with 10 earthquakes (including for co- 518
seismic), while significant enhancements in diurnal ratio are correlated with nine earthquakes out of ten 519
(including two post-seismic signatures). 520

521
522



Table 1: The following table summarizes the earthquake and its characteristics presence (Y) or absence (-) of potential enhancements in monofractal (f_D) and multifractal (h_w, f_{max}, h_{max}) components and diurnal ratio.

EQ. No.	Mag.	Foc. D.	Epi.D.	Single/Cluster	f_D	h_w	f_{max}	h_{max}	Diurnal ratio
1-45	-	Mod	Mod	C	-	Y	Co-	-	-
46-48	Mod	Mod	Mod	C	-	-	Y	Y	Y
49	Mod	Mod	Mod	S	Co-	Y	-	-	Y
50-51	Mod	Shallow/ Large	Large	C	Y	Y	-	-	Post-
52	Mod	Shallow	Large	S	-	-	-	-	Y
53-54-									
55	Large	Shallow	Small	C	Y	Y	Y	Y	Y
56	Mod	Mod	Large	S	Y	-	-	-	-
57	Large	Shallow	Large	S	Y	-	-	-	-
58	Large	Large	Mod	S	Y	-	-	-	-
59	Mod	Shallow	Large	S	-	-	-	-	Y
60	Mod	Large	Mod	S	Co-	-	-	-	Y
61	Mod	Shallow	Large	S	Co-	-	-	-	Y
62	Mod	Shallow	Large	S	-	-	-	-	-
63	Mod	Shallow	Large	S	-	-	-	-	post

According to Ida et al. (2012), significant enhancements in fractal values of geomagnetic signal recorded in tectonic active areas are representing the dominance of high frequency component associated with EM field from microfracturing processes in lithosphere. Apart from this, the components of holder exponent (part of multifractal analysis) such as f_{max} , h_{max} , h_{min} , and $h(0)$ also analyses the different characteristics of the signal (Krzyszczak et al., 2019) such as enhancement in h_{max} indicates that underlying process of events are more smooth rather than sorter fluctuations while h_{min} is just opposite to h_{max} . Similarly, f_{max} is correspond



to h_0 i.e. h which occurred maximum number of times in range $h_{max} - h_{min}$. The enhancements in f_{max} value 532
with large h indicate the underlying processes is less correlated and fine structure i.e. signal embedded with 533
anomalies and not completely regular while f_{max} correspond to smaller value of h indicate the highly 534
correlated and most regular signal. Enhancements in h_{max} and f_{max} with h_0 correspond to large h of a 535
geomagnetic signal recorded in active tectonic area, indicates that the underlying processes is smooth and 536
exhibit anomalies (less correlated and fine structures) of low frequencies. According to Conti et al. (2021) 537
electrokinetic process is responsible for generation of low frequency EM signature from lithospheric 538
deformation of a focal zone. 539

The enhancements in h_{max} and f_{max} , preceding the clusters of shallow earthquakes 1-45, 46-48, 53-55 on the 540
SS fault at moderate epicentral distances are indicative of low frequency perturbations from multiple sources, 541
which are ascribed to electrokinetic processes (Conti et al., 2021). For the cluster 50-51, the former occurs on 542
the SS fault and the latter on the WAF leading to interferences of the EM signals, whereby the h_{max} and f_{max} 543
enhancements are not prominent. 544

The earthquakes 49, 51 and 52 on the WAF dominated by strike slip mechanisms are also shallow and are at 545
moderate epicentral distances but have enhancements in f_D and h_w , the latter being more significant. This is 546
interpreted as high frequency perturbations attributed to microfracturing processes (Ida et al., 2012). 547

The earthquakes 56, 57, 59, 60, 61, 63 on the WAF and AT faults at large epicentral distances are linked with 548
enhancements in f_D and h_w , the former being more significant. We interpret these high frequency 549
perturbations to be also generated due to microfracturing processes; the large epicentral distances possibly 550
leading to attenuation of the highest frequency components leads to more prominent monofractal signatures. 551

The earthquakes 50, 58 and 62 are either at very large epicentral distances or large focal depths and fail to 552
produce signatures in any of the fractal components. 553



Thus, the moderate focal depth and epicentre distance earthquakes on WAF are dominated by h_w while large focal depth and epicentre distance earthquakes on WAF/AT dominated by f_D possibly indicating that the EM field from large distance are more homogeneous due to attenuation and dominating its appearance in f_D component, while EM field from short distance, indicating that EM field are more heterogeneous and dominating its appearance in h_w component. Which means, f_D component is most sensitive component for large epicentre and focal depth earthquakes while h_w component is more sensitive for moderate epicentre distance and focal depth earthquakes.

5. Conclusions

The study of fractal natures of the geomagnetic time series (Z component) allows us to conclude:

- (i) The earthquake clusters occurred on normal/thrust fault are of moderate magnitude and focal depth are emitting prior EM fields of low frequency effectively generated from electrokinetic processes in focal zone of earthquake.
- (ii) The single earthquakes occurred on strike slip WAF fault of moderate magnitude and focal depth are emitting prior EM field of more heterogeneity and frequency while, earthquakes on same fault with large epicentre distance/ focal depth emitting prior EM field of lesser heterogeneity and high frequency effectively generated from microfracturing processes in focal zone of earthquake.
- (iii) The monofractal dimension f_D is more effective to trace the EM field from large epicentre distance and focal depth while multifractal spectrum width h_w is more effective to trace the EM field from moderate to small epicentre distance and focal depth for the case of microfracturing processes.
- (iv) The fractal analysis has advantage over diurnal ratio is simultaneous observation of high and low frequency EM field from lithospheric deformation of focal zone of earthquake, which are emitted from different pre-earthquake processes.



Statements and Declarations	576
(i) Data Availability	577
	578
The data that support the findings of this study are available upon reasonable request.	579
	580
(ii) Competing Interests	581
	582
The authors have no relevant financial or non-financial interests to disclose.	583
	584
(iii) CRediT authorship contribution statement	585
	586
All authors contributed to the study conception and design. Methodology and data collection were performed by Kusumita Arora, and Rahul Prajapati. Data curation and its analysis using MATLAB coding was performed by Rahul Prajapati. The first draft of the manuscript was written by Rahul Prajapati. Review and editing of first draft of the manuscript performed by Kusumita Arora, and the work carried out under supervision and validation of Kusumita Arora. All authors read and approved the final manuscript.	587
	588
	589
	590
	591
	592
	593
Acknowledgments: The Authors are thankful to the Director CSIR-National Geophysical Research Institute, India for granting permission to access the data for research purpose and to publish the work (Ref. No. NGRI/Lib/2024/Pub-019). The authors acknowledge the available public domain data sets from WDC Kyoto (https://wdc.kugi.kyoto-u.ac.jp/) and earthquake data from ISC catalogue (http://www.isc.ac.uk/iscbulletin/search/catalogue/). Authors are also acknowledging the Dr. N. Phani Chandrasekhar and other observatories staff for maintaining the remote site observatories to acquire the uninterrupted data.	594
	595
	596
	597
	598
	599
	600
	601
	602
	603
	604



References

- Bak, P., Tang, C., and Wiesenfeld, K.: Self-organized criticality, *Phys. Rev. A*, 38, 364, 1988. 605
606
- Bella, J., Brodsky, B., and Berman, H. M.: Hydration structure of a collagen peptide, *Structure*, 3, 893–906, 607
1995. 608
- Bulusu, J., Arora, K., Singh, S., and Edara, A.: Simultaneous electric, magnetic and ULF anomalies associated
with moderate earthquakes in Kumaun Himalaya, *Nat. Hazards*, 1–31, 2023. 609
610
- Chadha, R. K., Singh, C., and Shekar, M.: Transient changes in well-water level in bore wells in Western India
due to the 2004 M W 9.3 Sumatra Earthquake, *Bull. Seismol. Soc. Am.*, 98, 2553–2558, 2008. 611
612
- Conti, L., Picozza, P., and Sotgiu, A.: A critical review of ground based observations of earthquake precursors,
Front. Earth Sci., 9, 676766, 2021. 613
614
- Crampin, S., McGonigle, R., and Bamford, D.: Estimating crack parameters from observations of P-wave
velocity anisotropy, *Geophysics*, 45, 345–360, 1980. 615
616
- Fraser-Smith, A. C., Bernardi, A., McGill, P. R., Ladd, M., Helliwell, R. A., and Villard Jr, O. G.: Low-
frequency magnetic field measurements near the epicenter of the Ms 7.1 Loma Prieta earthquake, *Geophys.*
Res. Lett., 17, 1465–1468, 1990. 617
618
619
- Gahalaut, V. K., Kundu, B., Laishram, S. S., Catherine, J., Kumar, A., Singh, M. D., Tiwari, R. P., Chadha,
R. K., Samanta, S. K., and Ambikapathy, A.: Aseismic plate boundary in the Indo-Burmese wedge, northwest
Sunda Arc, *Geology*, 41, 235–238, 2013. 620
621
622
- Gotoh, K., Akinaga, Y., Hayakawa, M., and Hattori, K.: Principal component analysis of ULF geomagnetic
data for Izu islands earthquakes in July 2000, *J. Atmos. Electr.*, 22, 1–12, 2002. 623
624
- Gotoh, K., Hayakawa, M., and Smirnova, N.: Fractal analysis of the ULF geomagnetic data obtained at Izu
Peninsula, Japan in relation to the nearby earthquake swarm of, *Natural Hazards and Earth System Sciences*,
229–236 pp., 2003. 625
626
627
- Han, P., Hattori, K., Xu, G., Ashida, R., Chen, C.-H., Febriani, F., and Yamaguchi, H.: Further investigations
of geomagnetic diurnal variations associated with the 2011 off the Pacific coast of Tohoku earthquake (Mw
9.0), *J. Asian Earth Sci.*, 114, 321–326, 2015. 628
629
630
- Han, P., Hattori, K., Huang, Q., Hirooka, S., and Yoshino, C.: Spatiotemporal characteristics of the
geomagnetic diurnal variation anomalies prior to the 2011 Tohoku earthquake (Mw 9.0) and the possible
coupling of multiple pre-earthquake phenomena, *J. Asian Earth Sci.*, 129, 13–21, 2016. 631
632
633
- Harris, S. K.: NATIONAL CENTER FOR EARTHQUAKE The Island of Guam Earthquake of, 1993. 634
- Hattori, K., Serita, A., Gotoh, K., Yoshino, C., Harada, M., Isezaki, N., and Hayakawa, M.: ULF geomagnetic
anomaly associated with 2000 Izu islands earthquake swarm, Japan, *Phys. Chem. Earth, Parts A/B/C*, 29, 425–
435, 2004a. 635
636
637



- Hattori, K., Takahashi, I., Yoshino, C., Isezaki, N., Iwasaki, H., Harada, M., Kawabata, K., Kopytenko, E., Kopytenko, Y., Maltsev, P., Korepanov, V., Molchanov, O., Hayakawa, M., Noda, Y., Nagao, T., and Uyeda, S.: ULF geomagnetic field measurements in Japan and some recent results associated with Iwateken Nairiku Hokubu earthquake in 1998, *Phys. Chem. Earth*, 29, 481–494, <https://doi.org/10.1016/j.pce.2003.09.019>, 2004b. 638–642
- Hattori, K., Han, P., Yoshino, C., Febriani, F., Yamaguchi, H., and Chen, C. H.: Investigation of ULF Seismo-Magnetic Phenomena in Kanto, Japan During 2000-2010: Case Studies and Statistical Studies, <https://doi.org/10.1007/s10712-012-9215-x>, 1 May 2013a. 643–645
- Hattori, K., Han, P., Yoshino, C., Febriani, F., Yamaguchi, H., and Chen, C.-H.: Investigation of ULF seismo-magnetic phenomena in Kanto, Japan during 2000–2010: case studies and statistical studies, *Surv. Geophys.*, 34, 293–316, 2013b. 646–648
- Hayakawa, M. and Molchanov, O. A.: Summary report of NASDA’s earthquake remote sensing frontier project, *Phys. Chem. Earth, Parts A/B/C*, 29, 617–625, 2004. 649–650
- Hayakawa, M., Kawate, R., Molchanov, O. A., and Yumoto, K.: Results of ultra-low-frequency magnetic field measurements during the Guam earthquake of 8 August 1993, *Geophys. Res. Lett.*, 23, 241–244, 1996. 651–652
- Hayakawa, M., Ito, T., and Smirnova, N.: Fractal analysis of ULF geomagnetic data associated with the Guam earthquake on August 8, 1993, *Geophys. Res. Lett.*, 26, 2797–2800, <https://doi.org/10.1029/1999GL005367>, 1999. 653–655
- Hayakawa, M., Itoh, T., Hattori, K., and Yumoto, K.: ULF electromagnetic precursors for an earthquake at Biak, Indonesia on February 17, 1996, *Geophys. Res. Lett.*, 27, 1531–1534, 2000. 656–657
- Hayakawa, M., Ida, Y. U. I., and Gotoh, K.: Multifractal analysis for the ULF geomagnetic data during the Guam earthquake, in: *IEEE 6th International Symposium on Electromagnetic Compatibility and Electromagnetic Ecology, 2005, Proceedings*, 239–243, <https://doi.org/10.1109/EMCECO.2005.1513113>, 2005. 658–661
- Hayakawa, M., Hattori, K., and Ohta, K.: Monitoring of ULF (ultra-low-frequency) Geomagnetic Variations Associated with Earthquakes, *Sensors*, 7, 1108–1122, 2007. 662–663
- He, P., Wen, Y., Xu, C., Liu, Y., and Fok, H. S.: New Evidence for Active Tectonics at the Boundary of the Kashi Depression , China , from Time Series InSAR Observations *Tectonophysics New evidence for active tectonics at the boundary of the Kashi Depression , China , from time series InSAR observations, Tectonophysics*, 653, 140–148, <https://doi.org/10.1016/j.tecto.2015.04.011>, 2015. 664–667
- Heavlin, W. D., Kappler, K., Yang, L., Fan, M., Hickey, J., Lemon, J., MacLean, L., Bleier, T., Riley, P., and Schneider, D.: Case-Control Study on a Decade of Ground-Based Magnetometers in California Reveals Modest Signal 24–72 hr Prior to Earthquakes, *J. Geophys. Res. Solid Earth*, 127, <https://doi.org/10.1029/2022JB024109>, 2022. 668–671
- Higuchi, T.: Approach to an irregular time series on the basis of the fractal theory, *Phys. D Nonlinear Phenom.*, 672



31, 277–283, 1988.	673
Ida, Y., Hayakawa, M., Adalev, A., and Gotoh, K.: Multifractal analysis for the ULF geomagnetic data during the 1993 Guam earthquake, <i>Nonlinear Process. Geophys.</i> , 12, 157–162, https://doi.org/10.5194/npg-12-157-2005 , 2005.	674 675 676
Ida, Y., Yang, D., Li, Q., Sun, H., and Hayakawa, M.: Detection of ULF electromagnetic emissions as a precursor to an earthquake in China with an improved polarization analysis, <i>Hazards Earth Syst. Sci.</i> , 775–777 pp., 2008.	677 678 679
Ida, Y., Yang, D., Li, Q., Sun, H., and Hayakawa, M.: Fractal analysis of ULF electromagnetic emissions in possible association with earthquakes in China, <i>Nonlinear Process. Geophys.</i> , 19, 577–583, https://doi.org/10.5194/npg-19-577-2012 , 2012.	680 681 682
Johnston, M. J. S., Mueller, R. J., Ware, R. H., and Davis, P. M.: Precision of geomagnetic field measurements in a tectonically active region, <i>J. Geomagn. Geoelectr.</i> , 36, 83–95, 1984.	683 684
Koizumi, N., Kitagawa, Y., Matsumoto, N., Takahashi, M., Sato, T., Kamigaichi, O., and Nakamura, K.: Preseismic groundwater level changes induced by crustal deformations related to earthquake swarms off the east coast of Izu Peninsula, Japan, <i>Geophys. Res. Lett.</i> , 31, 2004.	685 686 687
Kopytenko, Y. A., Matiashvili, T. G., Voronov, P. M., Kopytenko, E. A., and Molchanov, O. A.: Detection of ultra-low-frequency emissions connected with the Spitak earthquake and its aftershock activity, based on geomagnetic pulsations data at Dusheti and Vardzia observatories, <i>Phys. Earth Planet. Inter.</i> , 77, 85–95, 1993.	688 689 690
Krzyszczak, J., Baranowski, P., Zubik, M., Kazandjiev, V., Georgieva, V., Cezary, S., Siwek, K., Kozyra, J., and Nieróbca, A.: Multifractal characterization and comparison of meteorological time series from two climatic zones, 1811–1824, 2019.	691 692 693
Liu, J. Y., Tsai, Y. B., Chen, S. W., Lee, C. P., Chen, Y. C., Yen, H. Y., Chang, W. Y., and Liu, C.: Giant ionospheric disturbances excited by the M9.3 Sumatra earthquake of 26 December 2004, <i>Geophys. Res. Lett.</i> , 33, 2006.	694 695 696
Meng, J., Wang, C., Zhao, X., Coe, R., Li, Y., and Finn, D.: India-Asia collision was at 24 N and 50 Ma: palaeomagnetic proof from southernmost Asia, <i>Sci. Rep.</i> , 2, 925, 2012.	697 698
Molchanov, O. A. and Hayakawa, M.: Generation of ULF electromagnetic emissions by microfracturing, <i>Geophys. Res. Lett.</i> , 22, 3091–3094, https://doi.org/10.1029/95GL00781 , 1995.	699 700
Molchanov, O. A., Kopytenko, Y. A., Voronov, P. M., Kopytenko, E. A., Matiashvili, T. G., Fraser-Smith, A. C., and Bernardi, A.: Results of ULF magnetic field measurements near the epicenters of the Spitak (Ms= 6.9) and Loma Prieta (Ms= 7.1) earthquakes: Comparative analysis, <i>Geophys. Res. Lett.</i> , 19, 1495–1498, 1992.	701 702 703
Muzy, J.-F., Bacry, E., and Arneodo, A.: The multifractal formalism revisited with wavelets, <i>Int. J. Bifurc. Chaos</i> , 4, 245–302, 1994.	704 705
Ouzounov, D., Liu, D., Chunli, K., Cervone, G., Kafatos, M., and Taylor, P.: Outgoing long wave radiation	706



- variability from IR satellite data prior to major earthquakes, *Tectonophysics*, 431, 211–220, 2007. 707
- Panda, M. N., Mosher, C., and Chopra, A. K.: Application of wavelet transforms to reservoir data analysis and scaling, in: *SPE Annual Technical Conference and Exhibition*, 1996. 708 709
- Panda, S. K., Choudhury, S., Saraf, A. K., and Das, J. D.: MODIS land surface temperature data detects thermal anomaly preceding 8 October 2005 Kashmir earthquake, *Int. J. Remote Sens.*, 28, 4587–4596, 2007. 710 711
- Prajapati, R., Arora, A.: Investigation of geomagnetic field variations in search of seismo-electromagnetic emissions associated with earthquakes in subduction zone of Andaman-Nicobar, India, *Natural Hazards and Earth System Sciences*, under review. 712 713 714 715
- Potirakis, S. M., Hayakawa, M., and Schekotov, A.: Fractal analysis of the ground-recorded ULF magnetic fields prior to the 11 March 2011 Tohoku earthquake ($M_W = 9$): discriminating possible earthquake precursors from space-sourced disturbances, *Nat. Hazards*, 85, 59–86, <https://doi.org/10.1007/s11069-016-2558-8>, 2017. 716 717 718 719
- Rawat, G., Chauhan, V., and Dhamodharan, S.: Fractal dimension variability in ULF magnetic field with reference to local earthquakes at MPMGO, Ghuttu, *Geomatics*, *Nat. Hazards Risk*, 7, 1937–1947, <https://doi.org/10.1080/19475705.2015.1137242>, 2016. 720 721 722
- Rikitake, T.: Earthquake precursors, *Bull. Seismol. Soc. Am.*, 65, 1133–1162, 1975. 723
- Scholz, C. H., Sykes, L. R., and Aggarwal, Y. P.: Earthquake Prediction: A Physical Basis: Rock dilatancy and water diffusion may explain a large class of phenomena precursory to earthquakes., *Science* (80-.), 181, 803–810, 1973. 724 725 726
- Sethumadhav, M. S., Gunnell, Y., Ahmed, M. M., and Chinnaiyah: Late Archean manganese mineralization and younger supergene manganese ores in the Anmod-Bisgod region, Western Dharwar Craton, southern India: Geological characterization, palaeoenvironmental history, and geomorphological setting, *Ore Geol. Rev.*, 38, 70–89, <https://doi.org/10.1016/j.oregeorev.2010.06.001>, 2010. 727 728 729 730
- Smirnova, N., Hayakawa, M., and Gotoh, K.: Precursory behavior of fractal characteristics of the ULF electromagnetic fields in seismic active zones before strong earthquakes, *Phys. Chem. Earth, Parts A/B/C*, 29, 445–451, 2004. 731 732 733
- Smirnova, N. A., Kiyashchenko, D. A., Troyan, V. N., and Hayakawa, M.: Multifractal Approach to Study the Earthquake Precursory Signatures Using the Ground-Based Observations, *Review of Applied Physics*, Hayakawa and Ida, 2013. 734 735 736
- Stanica, D. A. and Stănică, D.: ULF pre-seismic geomagnetic anomalous signal related to Mw8.1 offshore chiapas earthquake, Mexico on 8 September 2017, *Entropy*, 21, <https://doi.org/10.3390/e21010029>, 2019. 737 738
- Turcotte, D. L.: Fractals in geology and geophysics, *Pure Appl. Geophys.*, 131, 171–196, 1989. 739



Uyeda, S., Hayakawa, M., Nagao, T., Molchanov, O., Hattori, K., Orihara, Y., Gotoh, K., Akinaga, Y., and 740
Tanaka, H.: Electric and magnetic phenomena observed before the volcano-seismic activity in 2000 in the Izu 741
Island Region, Japan, *Proc. Natl. Acad. Sci.*, 99, 7352–7355, 2002. 742

Virk, H. S., Walia, V., and Kumar, N.: Helium/radon precursory anomalies of Chamoli earthquake, Garhwal 743
Himalaya, India, *J. Geodyn.*, 31, 201–210, 2001. 744

Xu, G., Han, P., Huang, Q., Hattori, K., Febriani, F., and Yamaguchi, H.: Anomalous behaviors of 745
geomagnetic diurnal variations prior to the 2011 off the Pacific coast of Tohoku earthquake (Mw9.0), *J. Asian* 746
Earth Sci., 77, 59–65, <https://doi.org/10.1016/j.jseaes.2013.08.011>, 2013. 747

Yang, H., Pan, H., Wu, A., Luo, M., Konaté, A. A., and Meng, Q.: Application of well logs integration and 748
wavelet transform to improve fracture zones detection in metamorphic rocks, *J. Pet. Sci. Eng.*, 157, 716–723, 749
<https://doi.org/10.1016/j.petrol.2017.07.057>, 2017. 750

Yen, H.-Y., Chen, C.-H., Yeh, Y.-H., Liu, J.-Y., Lin, C.-R., and Tsai, Y.-B.: Geomagnetic fluctuations during 751
the 1999 Chi-Chi earthquake in Taiwan, *Earth Planets Space*, 39–45 pp., 2004. 752

753

754

755